Applied Catalysis B: Environmental 127 (2012) 212–220

Contents lists available at SciVerse ScienceDirect

Applied Catalysis B: Environmental

journal homepage: www.elsevier.com/locate/apcatb

Selective oxidation of glycerol with oxygen in base-free solution over MWCNTs supported PtSb alloy nanoparticles

Renfeng Nie[a], Dan Liang[a], Lian Shen[b], Jing Gao[a], Ping Chen[a], Zhaoyin Hou[a,*]

[a] Institute of Catalysis, Department of Chemistry, Zhejiang University, Hangzhou 310028, China
[b] College of Chemical Engineering and Materials Science, Zhejiang University of Technology, Hangzhou 310014, China

ARTICLE INFO

Article history:
Received 14 March 2012
Received in revised form 21 July 2012
Accepted 25 August 2012
Available online 31 August 2012

Keywords:
Glycerol oxidation
PtSb alloy, MWCNTs
Base-free
Dihydroxyacetone

ABSTRACT

Multiwall carbon nanotubes (MWCNTs) supported PtSb alloy nanoparticles were prepared and used in the selective oxidation of glycerol to dihydroxyacetone (DIHA) in a base-free aqueous solution. The structure and morphology of the prepared PtSb/MWCNTs catalyst were characterized and compared with that of Pt-Bi/MWCNTs. It was found that Sb homogenously entered into the lattice of Pt and PtSb alloy nanoparticles formed in PtSb/MWCNTs, but Pt particles in Pt-Bi/MWCNTs were wrapped by a layer of $Bi_2O_2CO_3$. PtSb/MWCNTs is extremely active for the selective oxidation of glycerol to DIHA. The turnover frequency of surface Pt atoms in PtSb/MWCNTs increased from 341.5 (of Pt/MWCNTs) to 878.1 h^{-1}. At the same time, DIHA is relatively 'stable' over the homogenous PtSb alloy nanoparticles, which also depressed the cleavage of C—C.

1. Introduction

Selective oxidation of polyols is a major topic in industrial petrochemical production. Many polyols oxidation processes are catalyzed by enzymes in order to reach valuable product selectivity [1–4]. Glycerol is the simplest triol with three hydrophilic hydroxyl groups. The rapidly rising production of biodiesel in United States and Europe has led to a drastic surplus of glycerol. Many biodiesel production facilities now view crude glycerol (typically containing 20% water and residual esterification catalyst) as waste, and current disposal of surplus glycerol is by incineration [5–9]. A lot of research works were reported in order to make value-added products from crude glycerol as an alternative to incineration [10,11].

One alternative route is the selective oxidation of glycerol to valuable oxygenated derivatives such as glyceric acid (GLYA), dihydroxyacetone (DIHA), hydroxypyruvic acid (HPYA) and tartronic acid (TARAC) [9–11]. But now, these oxygenated derivatives are produced either in costly and polluted chemical oxidation processes with lower selectivity (e.g., utilizing potassium permanganate, nitric acid or chromic acid as the oxidant) or in fermentation processes with low productivity [1–4,10,11]. Oxidation of an aqueous solution of glycerol using air and recyclable catalysts would provide a low-cost, environmental friendly route to these compounds [1–4].

In published papers, gold-based catalysts were reported and discussed in detail. It was found that Au/C catalyst was active for liquid-phase oxidation of glycerol to DIHA (26% selectivity) under atmospheric pressure when base was added in the reaction mixture (NaOH/glycerol > 2). However, the main product over Au/C catalysts was GLYA (up to 44%), and the conversion of glycerol depended strongly on base concentration and reaction time [12–28].

During the last decade, obvious progresses were reported in the selective oxidation of glycerol to GLYA [10–12,19,22]. Hutchings and co-workers found that the selectivity of GLYA reached 100% on Au/charcoal catalysts at a 54–56% conversion of glycerol when sodium hydroxide was added as a basic promoter [16–18]. Garcia et al. found that the selectivity to GLYA can be as high as 70% at 100% conversion of glycerol on Pd/C catalyst at pH 11 [28]. Rodrigues et al. found that the highest turnover frequency of Au on the surface of multiwall carbon nanotubes (MWCNTs) reached 5900 h^{-1} at NaOH/glycerol molar ratio = 2, 60 °C and 3 bar oxygen [29]. More recently, it was reported that Au-Pd/MgO [19], Au-Pt/H-mordenite [22], Pt/MWCNTs [30,31] and $PtCu_3$ alloy [32] were capable for the selective oxidation of glycerol to GLYA even in base-free solutions. But the selective oxidation of glycerol to DIHA in base-free solution is still a challenge. The progress in selective oxidation of glycerol to DIHA is slow, and mainly bismuth promoted Pt catalysts were tested and reported in published works [33–40].

Kimura et al. found that charcoal supported Pt catalysts showed a weak activity for selective oxidation of the secondary hydroxyl group of glycerol especially in an acidic media (pH 2–4) with a DIHA yield of 4% [33–35]. The catalytic performance of Pt could be improved when bismuth was used as a promoter, and it was

* Corresponding author. Tel.: +86 571 88273283; fax: +86 571 88273283.
E-mail address: zyhou@zju.edu.cn (Z. Hou).

0926-3373/$ – see front matter © 2012 Elsevier B.V. All rights reserved.
http://dx.doi.org/10.1016/j.apcatb.2012.08.026

Table 1
Composition and Pt dispersion.

Catalysts	Loading (wt.%)[a]			Pt dispersion (%)[b]	
	Pt	Bi	Sb	CO uptake (mmol/g_{-cata})	Dispersion (%)
Pt/MWCNTs	4.9	–	–	113.9	45.3
Pt-Bi/MWCNTs	4.6	5.2	–	126.1	53.4
PtSb/MWCNTs	3.8	–	3.0	106.9	54.8

[a] Determined by ICP.
[b] Calculated according to CO uptake.

found that the selectivity of DIHA increased from 10% to 80% at a low conversion of glycerol (20%) in a fixed-bed reactor [33–35]. In batch reactors, the highest yield of DIHA reached 37% at a 75% conversion of glycerol on carbon supported Pt-Bi catalyst [33–38]. Hu et al. disclosed that the secondary hydroxyl group in glycerol was preferentially oxidized on the surface of Pt-Bi nanoparticles and the formation rate of DIHA was high only at the beginning of reaction [39,40]. However, Pt-Bi also catalyzes further oxidation of formed DIHA and GLYA to a series of byproducts (such as oxalic acid and CO_2), and the selectivity of DIHA decreases quickly with the conversion of glycerol [39,40]. Kimura once postulated that bismuth adatoms function as site blockers on Pt (1 1 1), which controlled the glycerol orientation toward DIHA formation [33]. But the morphology of Bi promoted Pt catalyst is seldom characterized or presented in published works.

Recently, it was reported that micropore-free MWCNTs supported Pt [30–32,41] and Au [29,42–44] are more active for glycerol oxidation than active carbon supported Pt and Au catalysts. In this work, MWCNTs supported Sb-promoted Pt catalyst, which was extremely active for the selective oxidation of glycerol to DIHA in base-free condition, was prepared and reported for the first time. And its performance was compared with the popular reported Pt-Bi and monometallic Pt nanoparticles.

2. Experimental

2.1. Materials

MWCNTs with the diameter range of 20–45 nm that prepared by a conventional CVD method was purchased from Shenzhen Nanotech Port Co., Ltd. Metal salts, such as $H_2PtCl_6{\cdot}6H_2O$ (>99%), $BiCl_3$ (>99.99%) and Sb_2O_3 (>99.99%) were purchased from Sinopharm Chemical Reagent Co., Ltd (China). Glycerol (>99.0%), glyceric acid (40%, w/w in water), 1,3-dihydroxyacetone dimer (98%), glycolic acid (GLYCA, 98%), glyceraldehyde (GLYHD, 95%), hydroxypyruvic acid (HPYA, 95%), oxalic acid (OXALA, 98%) as well as reducing agent KBH_4 (≥98.0%) and $NH_2(CH_2)_2SH$ (>95.0%) were purchased from Alfa Aesar, SIGMA or TCI.

2.2. Catalyst preparation

2.2.1. Pretreatment of MWCNTs

Ten gram of MWCNTs was first immersed in 80 cm^3 HNO_3 (65–68 wt.%). The slurry was stirred and kept refluxing at 75 °C for 11 h. Then the solid was filtered out and washed with distilled water until the pH of eluent reached 6.5. The pretreated MWCNTs was dried in vacuum at 80 °C for 10 h and denoted as HNO_3-MWCNTs. Thiolation of the MWCNTs was performed via a method described in reference [45]. Five-gram HNO_3-MWCNTs was first chloridized via refluxing at 70 °C in 40 cm^3 $SOCl_2$ for 12 h, separated by filtration and washed with ethanol until free of Cl^-. And then the chloridized MWCNTs was further reacted with $NH_2(CH_2)_2SH$ in dehydrated toluene for 24 h. The prepared support was denoted as S-MWCNTs.

2.2.2. Metal loading

Pt/MWCNTs: An aqueous solution containing 0.01 g/cm^3 H_2PtCl_6 was added dropwise to a stirred suspension of 2.0 g S-MWCNTs. The slurry was stirred for 30 min at room temperature and sonicated for 2 h, reduced by an aqueous solution of KBH_4. And then it was filtered and washed with distilled deionized water to remove residual chlorine, which was checked with aqueous $AgNO_3$ solution. This catalyst, denoted as Pt/MWCNTs, was kept in moisture before use. Pt/MWCNTs was further treated in a H_2 gas flow for 1 h at 400 °C before reaction in order to eliminate the S-containing groups [31].

PtSb/MWCNTs: The above prepared Pt/MWCNTs (without heat-treatment in H_2) was further impregnated into a predetermined amount of Sb_2O_3 solution (dissolved in 12 M HCl), dried in vacuum, followed by hydrogen reduction at 400 °C and heat treatment at 500 °C in nitrogen flow (40 cm^3/min). PtSb bimetallic catalyst with a controlled Sb/Pt = 1 (mol ratio) is denoted as PtSb/MWCNTs.

Pt-Bi/MWCNTs: As a reference, Pt-Bi/MWCNTs catalyst was prepared via the further impregnation of Pt/MWCNTs (without heat-treatment in H_2) with an ethyl ether solution of $BiCl_3$, then dried in vacuum, followed by hydrogen reduction at 250 °C and heat treatment at 500 °C in nitrogen flow (40 cm^3/min). The derived Pt-Bi catalyst with a controlled Bi/Pt = 1 (mol ratio) is denoted as Pt-Bi/MWCNTs.

2.3. Characterization

Actual content of Pt, Sb and Bi in the prepared catalysts was determined on inductively coupled plasma-atomic emission spectroscopy (ICP, Plasma-Spec-II spectrometer) and these data were summarized in Table 1. Samples were first dissolved in aqua regia, and the mixtures were further oxidized with 30% hydrogen peroxide in order to make Pt dissolved completely. The dispersion of Pt was calculated on the basis of CO adsorption. Sample (0.15 g) was first pretreated in hydrogen (50 cm^3/min) at 150 °C for 1 h and purged with helium (50 cm^3/min) for 1 h at the same temperature. And then, the catalyst was cooled to room temperature and CO pulses were injected from a calibrated on-line sampling valve. CO adsorption was assumed to be completed after three successive peaks showed the same peak areas. A CO/Pt stoichiometry of 1 was used for calculations.

X-ray diffraction (XRD) was recorded on a RIGAKU D/MAX 2550/PC diffractometer using Cu Kα radiation at 40 kV and 100 mA. Diffraction data were recorded using continuous scanning at a rate of 0.02°/s and step 0.02°. The morphologies and dimensions of catalysts were observed on transmission electron microscopy (TEM) (JEOL-2010F) using an accelerating voltage of 200 kV. Pt, Sb and Bi (or $Bi_2O_2CO_3$) were identified by fast Fourier transforms (FFT) in high-resolution TEM analysis. Scanning transmission electron microscope and high-angle annular dark-field (STEM-HAADF) imaging was used to measure the individual nanoparticles with an aberration corrected FEI TECNAI G2 F30 S-TWIN (S)TEM operating at 300 kV, in addition with the capability of taking energy dispersive X-ray (EDX) spectra from individual particles larger than 1 nm. X-ray photoelectron spectra (XPS) were recorded on

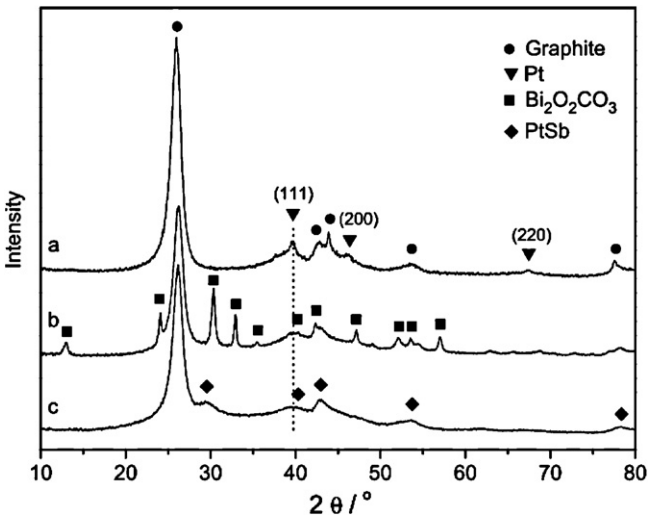

Fig. 1. XRD patterns of (a) Pt/MWCNTs, (b) Pt-Bi/MWCNTs and (c) PtSb/MWCNTs.

a Perkin–Elmer PHI ESCA System. X-ray source was Mg standard anode 146 (1253.6 eV) at 12 kV and 300 W. The binding energy was calibrated with respect to the C 1s level 284.20 eV of contaminated carbon.

2.4. Glycerol oxidation

Glycerol oxidation was performed in a three-neck flask (100 cm^3) equipped with gas supply system, magnetic stirrer, condenser and thermocouple. 50 cm^3 of 0.1 g/cm^3 glycerol solution and 0.5 g catalyst were added into the reactor. Once required temperature (60 °C) reached, O_2 (99.9%) was introduced into the reactor at 150 cm^3/min via a mass flow controller. After reaction, catalyst was filtered off and aqueous solution was charged into a 50 cm^3 volumetric flask and analyzed using an Agilent 1100 series high-performance liquid chromatography (HPLC) equipped with a G1314A Variable UV (210 nm) and a G1362A R.I. detector. Zorbax SAX column (4.6 mm × 250 mm, Agilent) was used with a mixed solution of H_3PO_4 (0.1%, w/w) in H_2O/acetonitrile (1/2, v/v) (1.0 cm^3/min) as the eluent at 25 °C. The reaction product samples were diluted 10 times with eluent before analysis. The amounts of consumed reactant and produced products were quantified with an external calibration method. During the oxidation reaction, gas in effluent was collected and analyzed using a TCD gas chromatograph equipped with an APS-201 (Flusin T) column. These procedures and the external calibration of each compound could be found in reference [31]. The turnover frequency (TOF) on the basis of surface Pt atom was calculated as: TOF = (number of glycerol molecular converted)/(number of surface Pt atoms)/(reaction time, h).

The selectivity of each product was calculated as: (mmol of product in reaction mixture) × (the number of carbon atoms in product)/((initial mmol of glycerol − mmol of glycerol left) × 3) × 100%.

Carbon balance was defined as: the total selectivity of DIHA, GLYHD, GLYA, HPYA and GLYCA. Others byproducts such as CO_2, CO and HCHO were detected in gas effluent and oxalic acid, HCOOH were detected in liquid phase.

3. Results and discussion

3.1. XRD analysis and Pt dispersion

Fig. 1 shows the XRD patterns of Pt/MWCNTs, Pt-Bi/MWCNTs and PtSb/MWCNTs prepared in this work. Beside the diffraction peaks of graphite, Pt is detected in monometallic Pt/MWCNTs (Fig. 1(a)), and the calculated Pt crystallite size on basis of the half-width of Pt (1 1 1) is 2.0 nm. Pt (1 1 1) reflex is very weak in PtSb/MWCNTs, while a newly formed PtSb alloy could be identified clearly at 29.8°, 41.5–43.8°, 53.9° and 78.9° [JCPDS 721440], which means that Sb homogenously entered into the lattice of Pt (Fig. 1(c)). On the other hand, mainly bismuth carbonate oxide ($Bi_2O_2CO_3$) is detected in Pt-Bi/MWCNTs [JCPDS 411488] and the diffraction peaks of Pt are faint (Fig. 1(b)). Similar XRD spectra of $Bi_2O_2CO_3$ and Pt were reported by Claus et al. on the surface of active carbon supported Pt-Bi catalysts [46]. The formation of separated $Bi_2O_2CO_3$ phase would depress the interaction between Bi and Pt in Pt-Bi/MWCNTs.

The dispersion of Pt atoms that calculated on the basis of CO adsorption is summarized in Table 1. It can be found that Pt dispersed highly on the surface of MWCNTs in all three catalysts. Sb further increased the dispersion of Pt from 45.3 (in Pt/MWCNTs) to 54.8% (in PtSb/MWCNTs), and this improvement would be attributed to the formation of PtSb alloy (see Fig. 1).

3.2. TEM images

Fig. 2 shows the typical TEM images of Pt/MWCNTs, Pt-Bi/MWCNTs, PtSb/MWCNTs with particle size distributions (top-right) and a typical STEM image of PtSb/MWCNTs. Highly dispersed Pt particles were detected in the TEM images of Pt/MWCNTs and the calculated average size of these particles is 2.0 nm, which fits well with that detected in XRD (Fig. 2(a)). But a broader size distribution ranged from 0.6 to 5.6 nm, along with a significant number of larger particles over 5.6 nm, appears in Pt-Bi/MWCNTs and the calculated average particle size increases to 3.49 nm (Fig. 2(b)). Though several bigger particles (sized in 3.8–5.0 nm) appear in PtSb/MWCNTs, no aggregated particle larger than 5.5 nm is detected (Fig. 2(c)) and the calculated average particle size is 2.75 nm. The highly dispersed PtSb alloy nanoparticles are also confirmed by STEM image that is shown in Fig. 2(d).

Fig. 3 shows the representative HR-TEM images of Pt-Bi nanoparticles in Pt-Bi/MWCNTs and PtSb alloy nanoparticles in PtSb/MWCNTs. It is quite interesting to find that the edge of Pt particles is wrapped by a layer of $Bi_2O_2CO_3$ (Fig. 3(a) and (b)). $Bi_2O_2CO_3$ locates mainly at the boundary between Pt particle and MWCNTs support, and the *d*-spacing values of 0.274 and 0.297 nm correspond to the (1 1 0) and (0 1 3) planes of $Bi_2O_2CO_3$ [JCPDS 411488], respectively. The outline of Pt crystalline lattice becomes faint and indistinct. While Pt and Sb distribute homogenously in the particles in PtSb/MWCNTs (Fig. 3(c–f)), no separated Pt or Sb lattice, or separated Pt or Sb cluster is detected. The *d*-spacing values of 0.219, 0.361 and 0.275 nm correspond to that of (1 0 2), (1 0 0) and (0 0 2) planes of PtSb alloy [JCPDS 721440], respectively. The outline and crystalline lattice of PtSb alloy are clear and distinct. These results indicate that the increased particle size of Pt-Bi nanoparticles (3.49 nm in average in Fig. 2(b)) in Pt-Bi/MWCNTs might be attributed to the coverage of $Bi_2O_2CO_3$ on the surface of Pt. On the other hand, the increased particle size of PtSb nanoparticles (2.75 nm in average in Fig. 2(c)) in PtSb/MWCNTs might be attributed to the formation of the homogenously dispersed PtSb alloy.

3.3. STEM images of PtSb/MWCNTs

In order to determine the fine structure of PtSb nanoparticles, STEM analysis was performed and those images are shown in Fig. 4. The HAADF images of a single PtSb alloy particle (Fig. 4(b)) shows that there is a good spatial correspondence of Pt and Sb elemental maps formed with the intensities of their L lines. At the same time, elemental linescans (Fig. 4(c)) across the PtSb alloy particle

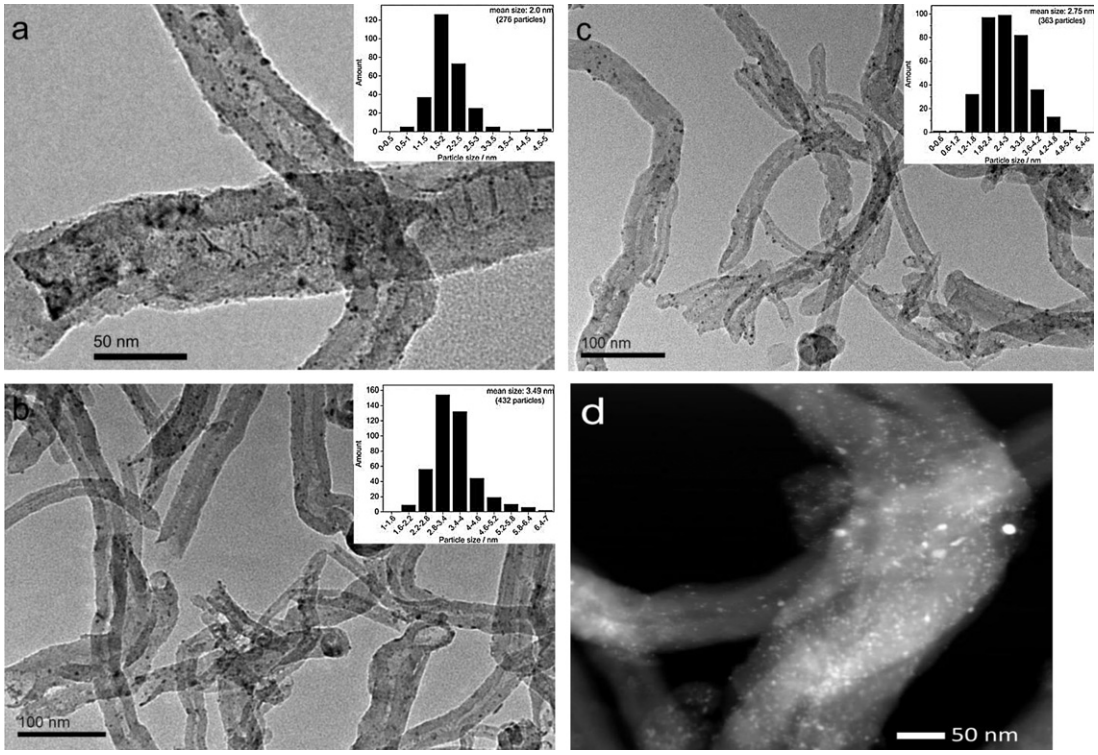

Fig. 2. TEM images of (a) Pt/MWCNTs, (b) Pt-Bi/MWCNTs, (c) PtSb/MWCNTs with particle size distributions (top-right), and (d) STEM image of PtSb/MWCNTs.

also suggest that the individual metal particles do contain both elements.

3.4. XPS analysis

XPS spectra of PtSb/MWCNTs and Pt-Bi/MWCNTs were collected in order to identify the structure and the electronic properties of Pt. As shown in Fig. 5(a), PtSb/MWCNTs exhibits a Pt 4f signal that can be deconvoluted into two pairs of doublets. The most intensive doublet with binding energies of 71.6 (Pt $4f_{7/2}$) and 74.8 eV (Pt $4f_{5/2}$) is attributed to metallic Pt. Peaks at 72.9 (Pt $4f_{7/2}$) and 76.4 eV (Pt $4f_{5/2}$) could be assigned to $Pt^{\delta+}$. It was found that 73.6% of the detected Pt atoms exist in metallic state and 26.4% in the form of $Pt^{\delta+}$ which might form during transfer of the sample in air to the XPS chamber (Table 2) [47,48]. The amounts of metallic Pt and $Pt^{\delta+}$ in Pt-Bi/MWCNTs catalyst are 59.6 and 40.4%, respectively (Fig. 5(c)).

Fig. 5(b) shows the XPS spectrum with peaks showing Sb 3d core level in PtSb/MWCNTs. The deconvolution of the Sb 3d core level reveals two chemical states of antimony, namely metallic Sb (528.9 eV (Sb $3d_{5/2}$) and 537.5 eV (Sb $3d_{3/2}$)) and Sb_2O_3 (530.56 eV (Sb $3d_{5/2}$) and 539.6 eV (Sb $3d_{3/2}$)), and the overlapping oxygen peak O 1s, at a binding energy of 532.08 eV. It was found that 71.1% of the Sb is in metallic state and 28.9% exists as Sb_2O_3 which also formed during transfer of the sample in air to the XPS chamber. This ratio fits well with that of $Pt/Pt^{\delta+}$, which further indicated that Pt and Sb dispersed homogenously in the PtSb alloy nanoparticles [48–50]. Bi 4f spectrum in Pt-Bi/MWCNTs can also be deconvoluted into two pairs of doublets (as shown in Fig. 5(d)). The doublet with binding energies of 157.1 eV (Bi $4f_{7/2}$) and 162.4 eV (Bi $4f_{5/2}$) is attributed to metallic Bi. Peaks at 158.8 (Bi $4f_{7/2}$) and 164.0 eV (Bi $4f_{5/2}$) could be assigned to Bi—O_x. And it was found that 43.4% of the detected Bi exists as metallic state and 56.6% exists as Bi—O_x (Table 2).

It can be found that the percentage of metallic Pt in PtSb/MWCNTs is higher than that of Pt-Bi/MWCNTs, which can be attributed to the formation of PtSb alloy (Fig. 1). The formation of separated $Bi_2O_2CO_3$ phase in Pt-Bi/MWCNTs would be derived from the strong interaction between Bi and the oxygen-containing groups on the surface of MWCNTs during heat treatment. And the formed $Bi_2O_2CO_3$ depressed the alloying of Bi and Pt, finally led to the formation $Bi_2O_2CO_3$ wrapped Pt particles. But alloying Pt with Sb in PtSb/MWCNTs can efficiently contribute the presence of as-reduced Pt and Sb. On the other hand, the homogenously doped Sb acts as a semiconductor which may be an appropriate promoter of Pt and hinders further oxidation of intermediate [51]. Another role of Sb promotion may be a geometric (blocking) effect which can also promote the selectivity of desired products on Pt.

According to the XRD spectra (Fig. 1), TEM images (Figs. 2 and 3), STEM linescans (Fig. 4) and XPS analyses (Fig. 5), we think that Sb homogenously entered into the lattice of Pt and PtSb alloy formed in PtSb/MWCNTs. But Pt particles in Pt-Bi/MWCNTs are embedded in $Bi_2O_2CO_3$. To the best of our memories, this is the first clear image of PtSb alloy nanoparticles in PtSb/MWCNTs. And the Bi embedded Pt particles in Pt-Bi/MWCNTs (Fig. 3(a) and (b)) also fit well with those suggestions (such as, Bi acts as a site block) in previous works [36–40]. According to these HRTEM images and STEM analyses, possible configurations of Pt-Bi nanoparticles and PtSb alloy nanoparticles on the surface of MWCNTs were illustrated in Fig. 6.

3.5. Glycerol oxidation in base-free solution

The performances of Pt/MWCNTs, PtSb/MWCNTs and Pt-Bi/MWCNTs for glycerol oxidation in a base-free aqueous solution at different conversion levels of glycerol (10, 50 and 90%) were summarized in Table 3. It can be found that GLYA is a major product (45.6% selectivity) on the surface of Pt/MWCNTs at the beginning of the oxidation (10% conversion of glycerol), and the calculated TOF on the basis of surface Pt atoms (Table 1) is 341.5 h^{-1}. Higher activity and substantial change in product distribution were observed when Pt/MWCNTs was modified with Bi and Sb. The calculated TOF

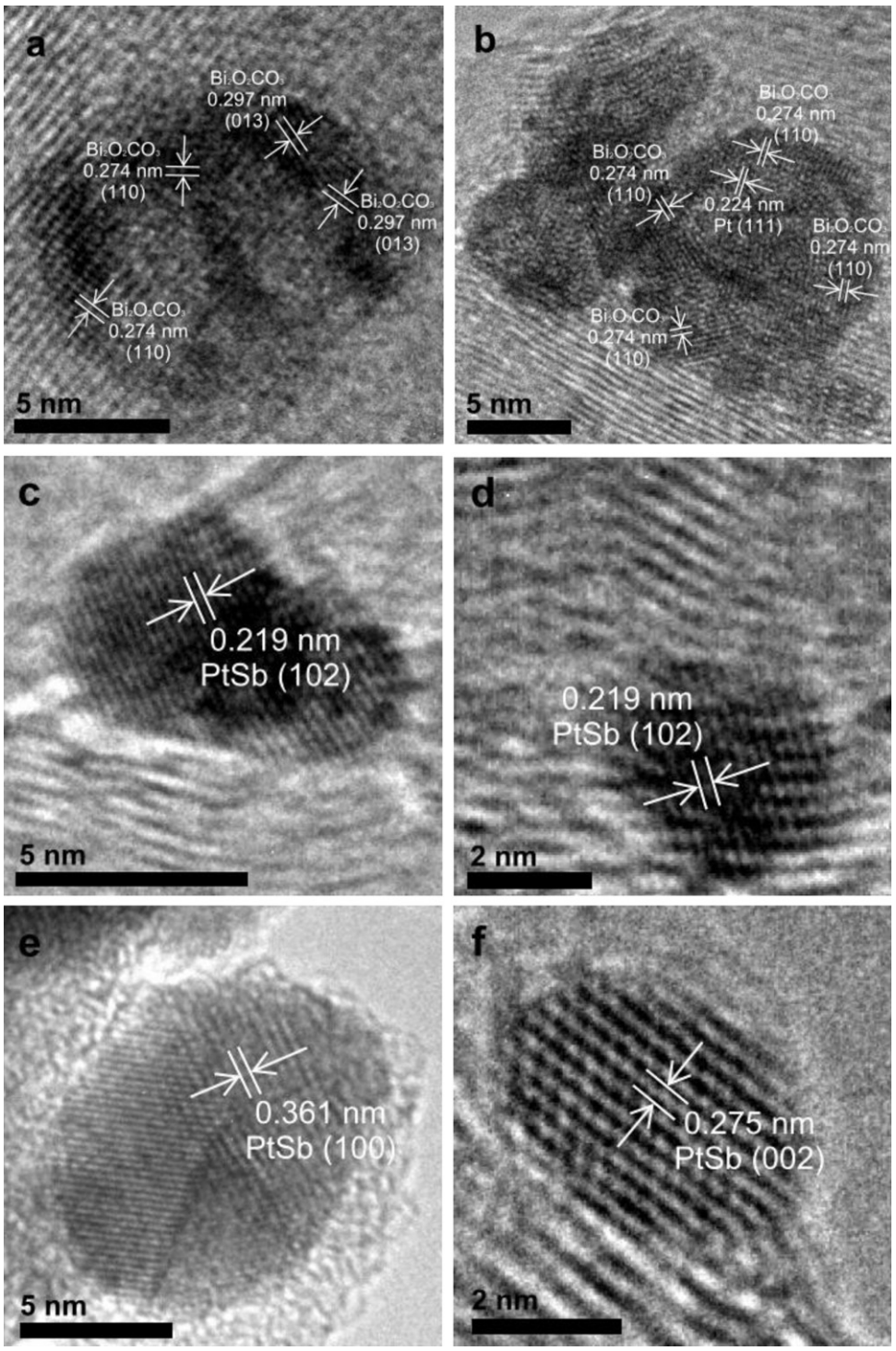

Fig. 3. HR-TEM images of (a and b) Pt-Bi NPs in Pt-Bi/MWCNTs and (c–f) PtSb alloy NPs in PtSb/MWCNTs.

Table 2
Surface composition of PtSb/MWCNTs and Pt-Bi/MWCNTs detected in XPS.

Catalysts	Surface mass concentration (%)						Relative atomic percentage (%)		
	C	O	Pt	Bi	Sb	S	$Pt^0/Pt^{\delta+}$	$Bi^0/Bi\text{-}O_x$	$Sb^0/Sb\text{-}O_x$
PtSb/MWCNTs	90.9	2.5	4.1	–	2.5	0.0	73.6/26.4	–	71.1/28.9
Pt-Bi/MWCNTs	87.5	3.8	4.8	3.9	–	0.0	59.6/40.4	43.4/56.6	–

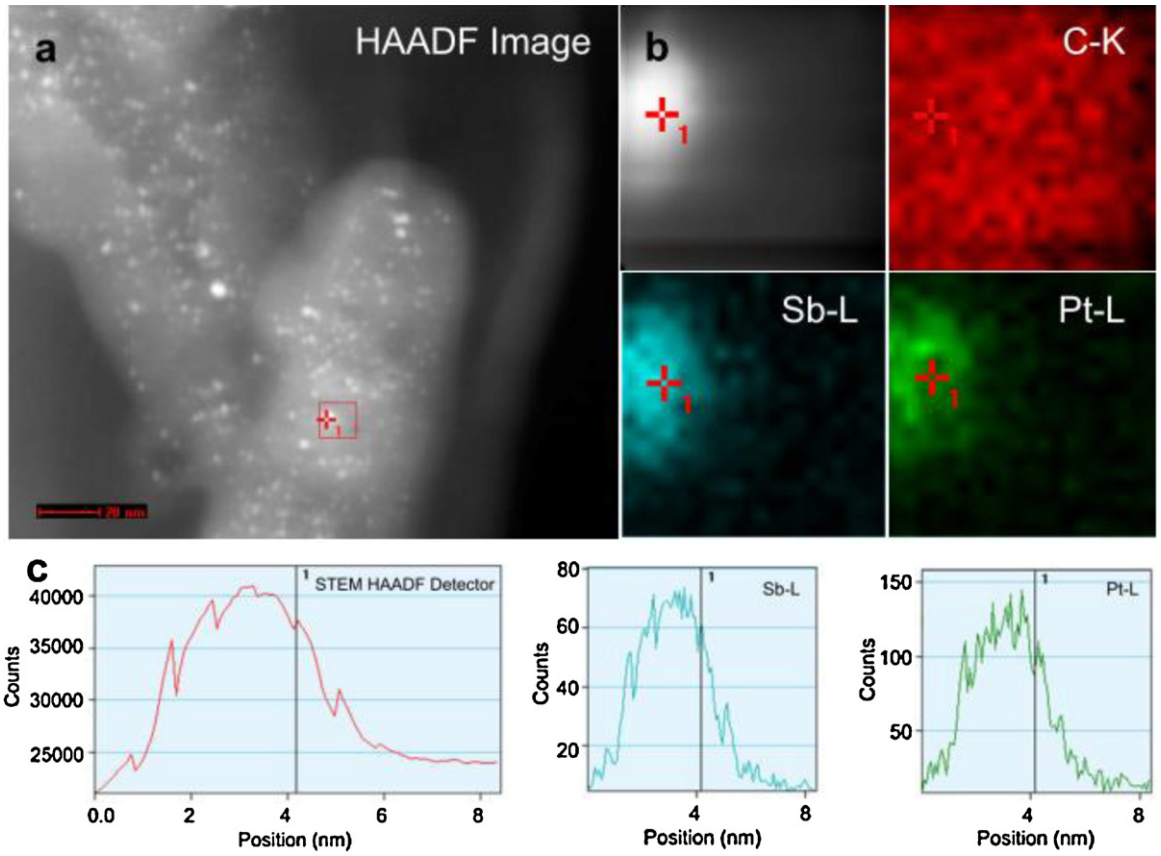

Fig. 4. STEM-HAADF images of PtSb/MWCNTs (a), along with the corresponding elemental maps (b) and linescans (c) from a single particle.

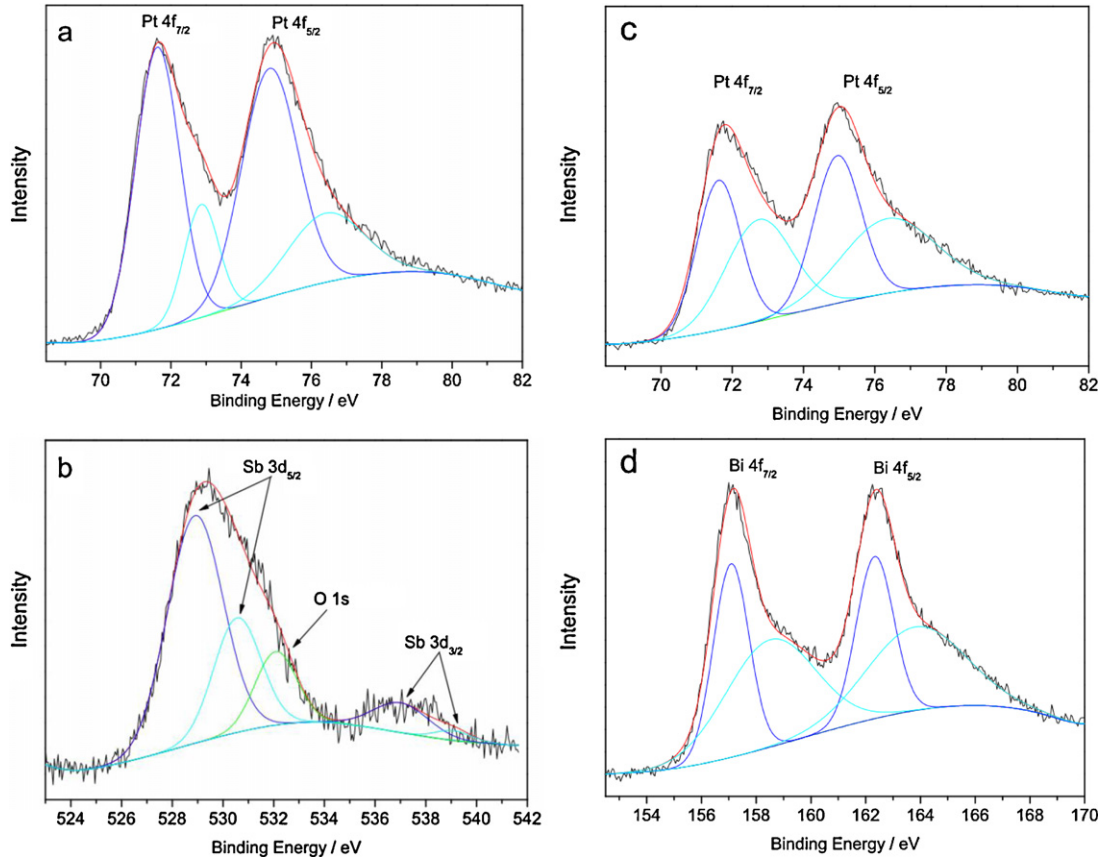

Fig. 5. XPS spectra of (a) Pt 4f, (b) Sb 3d in PtSb/MWCNTs, and (c) Pt 4f, (d) Bi 4f in Pt-Bi/MWCNTs.

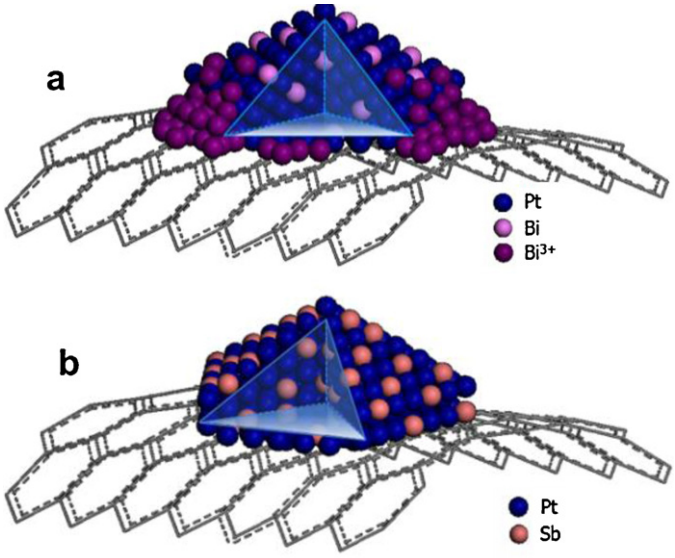

Fig. 6. Possible configurations of (a) Pt-Bi NPs, and (b) PtSb alloy NPs on MWCNTs.

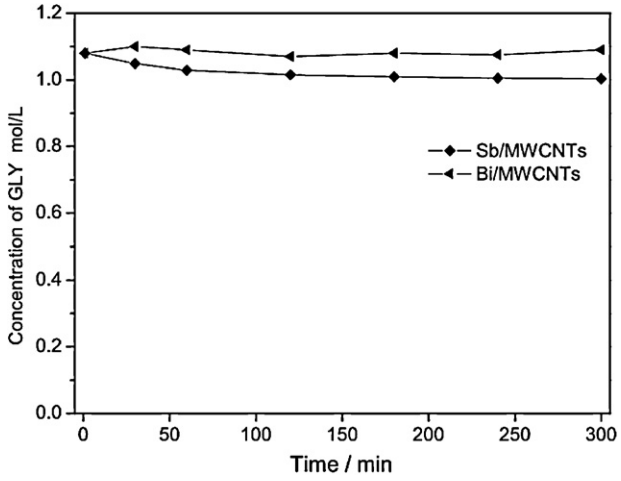

Fig. 7. Oxidation of glycerol over Bi/MWCNTs and Sb/MWCNTs. Reaction conditions: catalyst 0.5 g, 60 °C, oxygen 150 cm^3/min.

(at 10% conversion of glycerol) over Pt-Bi/MWCNTs on the basis of exposed Pt atoms increased to 500.8 h^{-1}, and the selectivity of DIHA reached 86.7%, but it decreased quickly to 51.1% at 50% conversion of glycerol and continuously decreased to 35.6% at 90% conversion of glycerol. These results could be attributed to that Pt-Bi also catalyzes the further oxidation of formed DIHA and GLYA to HPYA, GLYCA, and HPYA and GLYCA further decomposed easily to oxalic acid and CO_2 [33–40].

DIHA (with 80.8% selectivity) is the main product over PtSb/MWCNTs at the beginning of oxidation (10% conversion of glycerol), and the selectivity of DIHA decreased slowly to 67.5% (at 50% conversion of glycerol, see Table 3) and 51.4% (at 90% conversion of glycerol). At the same time, the TOF (at 10% conversion of glycerol) of PtSb/MWCNTs on the basis of surface Pt atoms reached 878.1 h^{-1}.

Meanwhile, another advantage of PtSb/MWCNTs catalyst which should be highlighted is that the serious C—C cleavage reaction over monometallic Pt/MWCNTs and Pt-Bi/MWCNTs is depressed. The combined selectivity of C1 and C2 (GLYCA, OXALA, others) decreased from 18.2% (on Pt/MWCNTs) and 2.6% (on Pt-Bi/MWCNTs) to 0.8% (on PtSb/MWCNTs) at low glycerol conversion (10%, see Table 3). Severe C—C cleavage happened over Pt-Bi/MWCNTs, as the combined selectivity of C1 and C2 increases quickly to 28.4% and 43.2% at 50% and 90% conversion of glycerol (see Table 3), but these values on PtSb/MWCNTs are 7.5 and 12.3%, respectively. These results indicate that PtSb alloy are more selective to DIHA than monometallic Pt and Pt-Bi nanoparticles. And the higher selectivity of GLYA on PtSb/MWCNTs than that of Pt-Bi/MWCNTs could also inhibit those kinds of active sites, which are predominantly responsible for the further oxidation of DIHA [33–40].

In order to make these suggestions clearly understood, the oxidation of glycerol over Bi/MWCNTs and Sb/MWCNTs, and stability of DIHA over Bi/MWCNTs, Sb/MWCNTs, Pt/MWCNTs, Pt-Bi/MWCNTs and PtSb/MWCNTs were investigated and shown in Figs. 7 and 8. It is found that no significant consumption of glycerol or DIHA could be detected over Bi/MWCNTs (Figs. 7 and 8(a)), which indicates that individual Bi is ineffective for these oxidation reactions, and the role of Bi would be a geometric (blocking) effect which decreases the size of Pt ensembles (as shown in Figs. 3(a and b) and 6). On the surface of Sb/MWCNTs (Figs. 7 and 8(a)), though a small amount of consumption is observed when glycerol fed as a reactant, DIHA appeared as a stable substrate and no obvious decrease is detected. That is, the oxidation reaction of glycerol and DIHA can also be negligible when single Sb/MWCNTs catalyst is used. Significant oxidations of DIHA were detected over Pt/MWCNTs, Pt-Bi/MWCNTs and PtSb/MWCNTs (Fig. 8(b)). But it appears that DIHA is relatively 'stable' over PtSb/MWCNTs. These

Table 3
The performance for selective oxidation of glycerol.[a]

Catalysts	Conversion (%)	TOF (h^{-1})[b]	Selectivity (%)[c]					
			DIHA	GLYA	GLYHD	HPYA	GLYCA	Carbon balance[d]
Pt/MWCNTs	10	341.5	20.6	45.6	2.8	12.8	5.4	87.2
	50	214.0	17.3	60.2	2.6	0.0	4.0	84.1
	90	164.8	12.6	67.4	1.6	0.0	3.5	85.1
Pt-Bi/MWCNTs	10	500.8	86.7	9.7	0.0	1.0	0.0	97.4
	50	276.7	51.1	11.1	2.3	7.1	2.7	74.3
	90	172.6	35.6	15.9	1.9	3.4	5.5	62.3
PtSb/MWCNTs	10	878.1	80.8	15.0	1.3	2.1	0.0	99.2
	50	498.2	67.5	18.9	2.5	3.6	4.5	97.0
	90	229.0	51.4	28.4	2.4	5.5	2.9	90.6

[a] Reaction conditions: 50 mL glycerol aqueous solution (0.1 g/mL), 0.5 g catalyst, 60 °C, O_2, 150 cm^3/min.
[b] TOF = (number of glycerol moleculars converted)/(number of surface Pt atoms)/(reaction time, h).
[c] Selectivity was calculated as: (mmol of product in reaction mixture) × (the number of carbon atom in product)/((initial mmol of glycerol − mmol of glycerol left) × 3) × 100%. DIHA: 1,3-dihydrooxyacetone, GLYA: glyceric acid, GLYHD: glyceraldehydes, HPYA: hydroxypyruvic acid, GLYCA: glycolic acid.
[d] Carbon balance = the total selectivity of DIHA, GLYHD, GLYA, HPYA and GLYCA, others byproducts such as CO_2, CO and HCHO were detected in gas effluent and oxalic acid, HCOOH were detected in liquid phase.

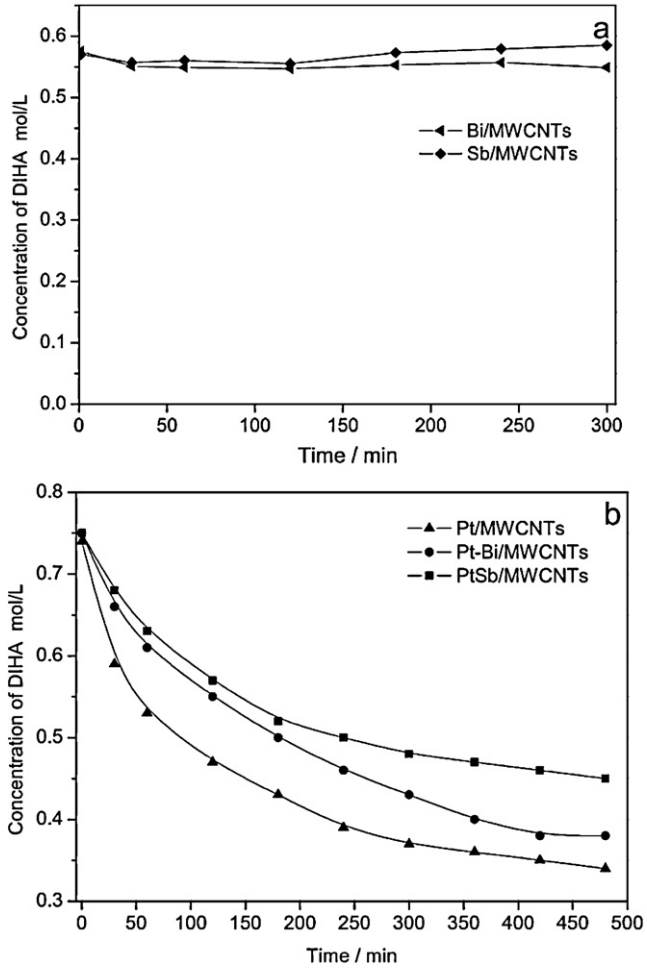

Fig. 8. Stability of DIHA over Bi/MWCNTs, Sb/MWCNTs (a), and Pt/MWCNTs, Pt-Bi/MWCNTs, PtSb/MWCNTs (b). Reaction conditions: catalyst 0.5 g, 60 °C, oxygen 150 cm^3/min.

results indicated that the formed DIHA consumed readily on Pt-Bi and serious C—C cleavage happened with the increasing conversion of glycerol (see Table 3), which decreased the selectivity of DIHA (as shown in Fig. 9(a)). On the other hand, DIHA is relatively 'stable' over PtSb/MWCNTs and the C—C cleavage is depressed (as shown in Fig. 9(b)).

According to above characterizations, the higher activity of PtSb/MWCNTs could attributed to the formation of PtSb alloy (see Fig. 1) and Pt dispersed highly (see Table 1). Previous works found that the activity of Pt for glycerol oxidation increased with the decreasing particle size of Pt [30–32,41,52,53].

During the oxidation of glycerol, previous works found that the formation of GLYA proceeded easily on monometallic Pt [30–32]. After introducing Bi to Pt, Hu et al. found that the formation of DIHA is more favorable than the formation of GLYA [39,40]. This promotion was postulated as bismuth adatoms function as site blockers on Pt (1 1 1) that controlled the glycerol orientation toward DIHA formation [33]. But Bi promoted Pt catalyst is also active for the deep oxidation of DIHA and GLYA to HPYA, GLYCA, and HPYA and GLYCA further decomposed easily to oxalic acid and CO_2 (see Fig. 9(a)).

In this work, the increased selectivity of DIHA over PtSb/MWCNTs might be attributed to the following possible reasons. (1) Homogenously added Sb in PtSb alloy acts as a semiconductor which may be an appropriate promoter of Pt and hinders further oxidation of intermediate (see XPS analysis in Fig. 5) [51]. (2) Sb atom in PtSb alloy is a more efficient site blocker on Pt that enhanced the formation of DIHA (Fig. 6). (3) Homogenously dispersed PtSb is less active for the further oxidation of DIHA (see Fig. 8). At the same time, this enhanced selectivity could also be contributed to the selectivity of GLYA on PtSb/MWCNTs is higher than that on Pt-Bi/MWCNTs (see Table 3), because GLYA favors to inhibit those kinds of active sites which are predominantly responsible for the further oxidation of DIHA [36].

On the basis of above experiments and discussion, the reaction networks of glycerol oxidation over Pt-Bi/MWCNTs and PtSb/MWCNTs were proposed in Fig. 9. In brief, DIHA and GLYHD are primary products in glycerol oxidation process, and the formation of DIHA is more favorable than GLYHD on both catalysts [39,40]. The further oxidation of DIHA and GLYA to HPYA, GLYCA, oxalic acid and CO_2 proceeded quickly on Pt-Bi/MWCNTs. But these deep oxidations were partially depressed on PtSb alloy because of the four reasons discussed in above paragraph.

Fig. 10 shows the conversion of glycerol, the selectivity of DIHA and GLYA over recycled PtSb/MWCNTs catalyst. These reactions were performed at 60 °C and reaction time of 2 h, catalyst was separated by centrifugation and washed with water for 5 times before another reaction. It can be found that the conversion of glycerol, the selectivity of DIHA and GLYA on fresh PtSb/MWCNTs catalyst were 66.2, 62.7 and 23.3%, respectively. The conversion of glycerol decreased slightly to 63.5% in the 5th recycle, but the selectivity of DIHA and GLYA remained stable. These results indicated

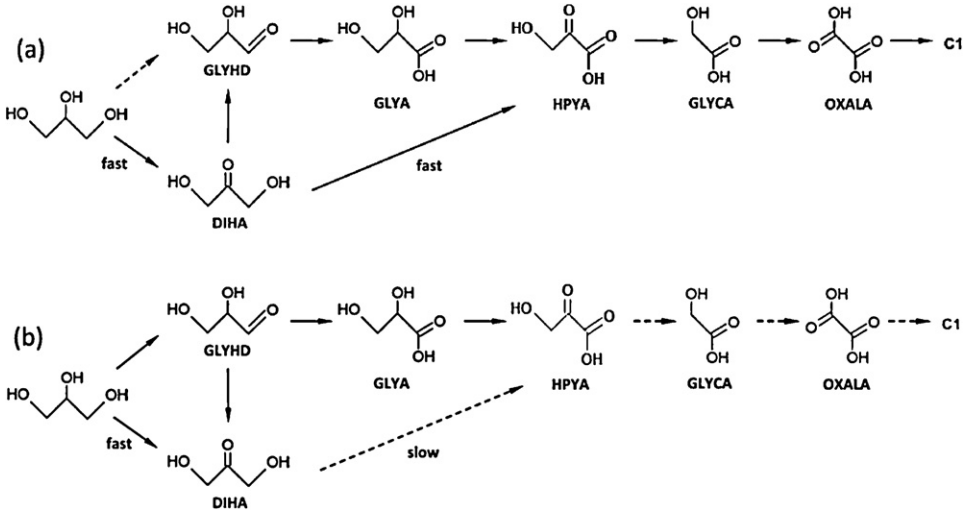

Fig. 9. Reaction networks of selective oxidation of glycerol over (a) Pt-Bi/MWCNTs and (b) PtSb/MWCNTs.

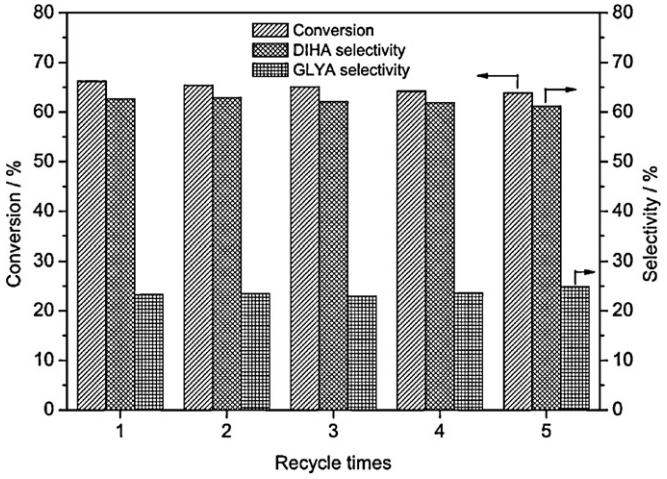

Fig. 10. The performance of recycled PtSb/MWCNTs. (Reaction conditions: 50 cm^3 glycerol aqueous solution (0.1 g/cm^3), 60 °C, O_2 150 cm^3/min, 2 h.)

this catalyst is stable and selective for the oxidation of glycerol to DIHA.

4. Conclusion

Unique sized and homogenously dispersed PtSb alloy nanoparticles were prepared on the surface of S-pretreated MWCNTs, and this catalyst was highly active and more efficient than monometallic Pt/MWCNTs and Pt-Bi/MWCNTs toward the selective oxidation of glycerol to DIHA in a base-free aqueous solution. Analysis disclosed that remarkable differences in catalytic behavior for glycerol oxidation between PtSb/MWCNTs and Pt-Bi/MWCNTs can be attributed to their different structures. And DIHA is relatively 'stable' over the homogenous PtSb alloy nanoparticles, which also depressed the cleavage of C—C.

Acknowledgments

This work was financially supported by the National Natural Science Foundation of China (Contract No. 21073159), Natural Science Foundation of Zhejiang Province (Grant No. LZ12B030001) and the Pre-research Ocean Foundation of Zhejiang University (2012HY025B).

References

[1] X.L. Chen, Y.G. Zheng, Y.C. Shen, Chemical Reviews 107 (2007) 1777–1830.
[2] C.H. Zhou, J.N. Beltramini, Y.X. Fan, G.Q. Lu, Chemical Society Reviews 37 (2008) 527–549.
[3] M.G. Musolino, L.A. Scarpino, F. Mauriello, R. Pietropaolo, ChemSusChem 4 (2011) 1143–1150.
[4] B.H. Shanks, Industrial and Engineering Chemistry Research 49 (2010) 10212–10217.
[5] D.R. Dodds, R.A. Gross, Science 318 (2007) 1250–1251.
[6] S.H. Chai, H.P. Wang, Y. Liang, B.Q. Xu, Green Chemistry 9 (2007) 1130–1136.
[7] S.H. Chai, H.P. Wang, Y. Liang, B.Q. Xu, Journal of Catalysis 250 (2007) 342–349.
[8] J.J. Bozell, Science 329 (2010) 522–523.
[9] J.J. Bozell, G.R. Petersen, Green Chemistry 12 (2010) 539–554.
[10] M. Pagliaro, R. Ciriminna, H. Kimura, M. Rossi, C.D. Pina, Angewandte Chemie International Edition 46 (2007) 4434–4440.
[11] B. Katryniok, H. Kimura, E. Skrzynska, J.S. Girardon, P. Fongarland, M. Capron, R. Ducoulombier, N. Mimura, S. Paul, F. Dumeignil, Green Chemistry 13 (2011) 1960–1979.
[12] B.N. Zope, D.D. Hibbitts, M. Neurock, R.J. Davis, Science 330 (2010) 70–74.
[13] B.N. Zope, R.J. David, Topics in Catalysis 52 (2009) 269–277.
[14] W.C. Ketchie, Y.L. Fang, M.S. Wong, M. Murayama, R.J. Davis, Journal of Catalysis 250 (2007) 94–101.
[15] E.P. Maris, W.C. Ketchie, M. Murayama, R.J. Davis, Journal of Catalysis 251 (2007) 281–294.
[16] S. Carrettin, P. McMorn, P. Johnston, K. Griffin, C.J. Kiely, G.J. Hutchings, Physical Chemistry Chemical Physics 5 (2003) 1329–1336.
[17] S. Carrettin, P. McMorn, P. Johnston, K. Griffin, G.J. Hutchings, Chemical Communications 7 (2002) 696–697.
[18] S. Pollington, D.I. Enache, P. Landon, S. Meenakshisundaram, N. Dimitratos, A. Wagland, G.J. Hutchings, E.H. Stitt, Catalysis Today 145 (2009) 169–175.
[19] G.L. Brett, Q. He, C. Hammond, P.J. Miedziak, N. Dimitratos, M. Sankar, A.A. Herzing, M. Conte, J.A. Lopez-Sanchez, C.J. Kiely, D.W. Knight, S.H. Taylor, G.J. Hutchings, Angewandte Chemie International Edition 50 (2011) 10136–10139.
[20] F. Porta, L. Prati, Journal of Catalysis 224 (2004) 397–403.
[21] L. Prati, P. Spontoni, A. Gaiassi, Topics in Catalysis 52 (2009) 288–296.
[22] A. Villa, G.M. Veith, L. Prati, Angewandte Chemie International Edition 49 (2010) 4499–4502.
[23] A. Villa, A. Gaiassi, I. Rossetti, C.L. Bianchi, K.V. Benthem, G.M. Veith, L. Prati, Journal of Catalysis 275 (2010) 108–116.
[24] A. Villa, C. Campione, L. Prati, Catalysis Letters 115 (2007) 133–136.
[25] D. Wang, A. Villa, F. Porta, D.S. Su, L. Prati, Chemical Communications (2006) 1956–1958.
[26] P. Fordham, M. Besson, P. Gallezot, Applied Catalysis A 133 (1995) L179–L184.
[27] P. Fordham, M. Besson, P. Gallezot, Catalysis Letters 46 (1997) 195–199.
[28] R. Garcia, M. Besson, P. Gallezot, Applied Catalysis A 127 (1995) 165–176.
[29] E.G. Rodrigues, S.A.C. Carabineiro, J.J. Delgado, X. Chen, M.F.R. Pereira, J.J.M. Órfão, Journal of Catalysis 285 (2012) 83–91.
[30] J. Gao, D. Liang, P. Chen, Z.Y. Hou, X.M. Zheng, Catalysis Letters 130 (2009) 185–191.
[31] D. Liang, J. Gao, H. Sun, P. Chen, Z.Y. Hou, X.M. Zheng, Applied Catalysis B 106 (2011) 423–432.
[32] D. Liang, J. Gao, J.H. Wang, P. Chen, Y.F. Wei, Z.Y. Hou, Catalysis Communications 12 (2011) 1059–1062.
[33] H. Kimura, K. Tsuto, T. Wakisaka, Y. Kazumi, Y. Inaya, Applied Catalysis A 96 (1993) 217–228.
[34] H. Kimura, Polymers for Advanced Technologies 12 (2001) 697–710.
[35] H. Kimura, Applied Catalysis A 105 (1993) 147–158.
[36] N. Wörz, A. Brandner, P. Claus, Journal of Physical Chemistry C 114 (2010) 1164–1172.
[37] S. Demirel, K. Lehnert, M. Lucas, P. Claus, Applied Catalysis B 70 (2007) 637–643.
[38] S. Demirel, P. Kern, M. Lucas, P. Claus, Catalysis Today 122 (2007) 292–300.
[39] W.B. Hu, B. Lowry, A. Varma, Applied Catalysis B 106 (2011) 123–132.
[40] W.B. Hu, D. Knight, B. Lowry, A. Varma, Industrial and Engineering Chemistry Research 49 (2010) 10876–10882.
[41] Z.Y. Lin, H.B. Chu, Y.H. Shen, L. Wei, H.C. Liu, Y. Li, Chemical Communications 46 (2009) 7167–7169.
[42] E.G. Rodrigues, M.F.R. Pereira, J.J. Delgado, X. Chen, J.J.M. Órfão, Catalysis Communications 16 (2011) 64–69.
[43] E.G. Rodrigues, M.F.R. Pereira, X. Chen, J.J. Delgado, J.J.M. Órfão, Journal of Catalysis 281 (2011) 119–127.
[44] E.G. Rodrigues, S.A.C. Carabineiro, X. Chen, J. Delgado, J.L. Figueiredo, M.F.R. Pereira, J.M. Órfão, Catalysis Letters 141 (2011) 420–431.
[45] Y.T. Kim, K. Ohshima, K. Higashimine, T. Uruga, M. Takata, H. Suematsu, T. Mitani, Angewandte Chemie International Edition 45 (2006) 407–411.
[46] A. Brandner, K. Lehnert, A. Bienholz, M. Lucas, P. Claus, Topics in Catalysis 52 (2009) 278–287.
[47] R.F. Nie, J.H. Wang, L.N. Wang, Y. Qin, P. Chen, Z.Y. Hou, Carbon 50 (2012) 586–596.
[48] J.H. Kim, S.M. Choi, S.H. Nam, M.H. Seo, S.H. Choi, W.B. Kim, Applied Catalysis B 82 (2008) 89–102.
[49] X.L. Ji, K.T. Lee, R. Holden, L. Zhang, J.J. Zhang, G.A. Botton, M. Couillard, L.F. Nazar, Nature Chemistry 2 (2010) 286–293.
[50] J. Després, M. Elsener, M. Koebel, O. Kröcher, B. Schnyder, A. Wokaun, Applied Catalysis B 50 (2004) 73–82.
[51] Y.S. Kim, H.S. Jang, W.B. Kim, Journal of Materials Chemistry 20 (2010) 7859–7863.
[52] D. Liang, J. Gao, J.H. Wang, P. Chen, Z.Y. Hou, X.M. Zheng, Catalysis Communications 10 (2009) 1586–1590.
[53] D. Liang, S.Y. Cui, J. Gao, J.H. Wang, P. Chen, Z.Y. Hou, Chinese Journal of Catalysis 32 (2011) 1831–1837.